Desalination and Water Treatment
www.deswater.com

doi: 10.5004/dwt.2020.25187

188 (2020) 223–231
June

Removal of Cr(III) from aqueous solutions using waste kelp-derived biochar

Ning Zhao[a,b], Haiming Huang[a,*], Xiaomei Lv[a], Jing Li[a,b], Guojun Guo[a,b], Yulei Liu[a]

[a]*School of Environment and Civil Engineering, Dongguan University of Technology, Dongguan 523808, China, email: huanghaiming52hu@163.com*
[b]*Hebei Key Laboratory of Applied Chemistry, School of Environmental and Chemical Engineering, Yanshan University, Qinhuangdao 066004, China*

Received 6 June 2019; Accepted 15 November 2019

ABSTRACT

This study aimed to investigate the feasibility of using biochar derived from waste kelp biochar (KB) to remove Cr(III) from aqueous solutions. Scanning electron microscopy-energy-dispersive X-ray spectroscopy analysis revealed that KB could successfully adsorb Cr(III), while Fourier transforms infrared spectroscopy characterization suggested that electrostatic interaction was the major mechanism for the adsorption of Cr(III) on KB. Kinetic and isotherm studies on Cr(III) adsorption revealed that the pseudo-second-order kinetic model and the Langmuir model could adequately explain the adsorption of Cr(III) on KB. The maximum adsorption capacity of KB for Cr(III) was found to be 39.16 mg/g, while 91.13% of Cr(III) removal could be achieved by adding KB to aqueous solutions with an initial Cr(III) concentration of 25 mg/L at 0.9 g/L. Our experiments on cation competition demonstrated that the presence of Ca^{2+} could markedly inhibit the adsorption of Cr(III) by KB, although the inhibition was not observed with the presence of K^{+}, Na^{+}, and Mg^{2+} in the solution. When monovalent anions such as $C_5H_7O_5COO^{-}$ and CH_3COO^{-} were present in the solution, they reacted with Cr(III) to form stable complexes, thereby reducing the removal efficiency of Cr(III). On the other hand, the . of PO_4^{3-} and SO_4^{2-} did not cause any inhibition in the adsorption of Cr(III).

Keywords: Chromium removal; Biochar; Waste kelp; Adsorption

1. Introduction

Heavy metal pollution in water bodies has a critical negative impact of human activities on the environment, which is rapidly expanding with the rapid development of the human economy [1]. This type of pollution not only harms the environment but also human health. For instance, the valence of chromium (Cr) mainly contains 2 species of trivalent Cr(III) and hexavalent Cr(VI), which can mutually convert each other in the environment. They are both harmful to human health. Cr(III) has a teratogenic effect, while Cr(VI) is nearly 300-times more carcinogenic, mutagenic, and toxic than Cr(III) [2]. Chromium possesses the features of accumulation and biologic chain concentration, and therefore it can migrate to the soil in an ionic state and accumulate among various organisms such as vegetables and seafood [3]. As a result, Cr can easily bio-enrich into animals and plants, and, subsequently, enter the human body, endangering human health. Hence, it is extremely necessary to remove heavy metals from wastewaters before discharging it into the environment.

Various processes, including chemical [4], physical [5], and biological [6], have been applied to remove heavy metals from polluted water. Among these, biosorption techniques are the most common and cost-effective ones, which can be attributed to the fact that biological adsorbents are environment-friendly and abundant [7]. One of the most popular biological adsorbents is biochar—a material generated from biomass after pyrolysis [8,9]. Biochar offers the advantages

* Corresponding author.

of (i) low-cost, (ii) wide range of materials, (iii) high porosity, (iv) large specific surface area, and (v) thermal stability [1,9] for usage. In addition, biochar is almost similar to pure carbon. When adsorbed saturated biochar is scientifically buried underground, it does not disappear for hundreds of thousands of years, which indicates that carbon sequestration into the soil helps slow down the phenomenon of global warming. Owing to these advantages, biochar has aroused the widespread interest of researchers. In recent years, various raw materials have been used for preparing biochar and removing heavy metals. Agricultural wastes such as wood [10], straw [11], and pericarp [12] are the most commonly used raw materials for biochar. Furthermore, sewage sludge [13,14], chestnut shells [15], yak manure biochar [16], and marine macro-algae [17] also serve as raw materials for preparing biochar. Since the surface of biochar derived from marine macro-algae has a high pH value and various oxygen-containing functional groups, it is considered to possess a high potential for adsorbing cationic heavy metals from aqueous solutions [17]. China is one of the most abundant marine algae resources in the world. Large-scale exploitation and the utilization of algae, in processes such as food, cosmetics, and chemical production, originated in the 1950s and 1960s. Incidentally, marine macro-algae are widespread on a large scale. There are many un-fresh, abandoned marine macro-algae that are difficult to dispose. It would thus be of great significance to transform these raw, abandoned marine macro-algae into renewable resources. Not only in China, Japan and Korea also have marine algae-producing. Especially in Korea, it was reported that nearly 68,000 tons amount of algae in 2016 were obtained producing a lot of waste [17]. In addition, due to the growing environment and flaky fiber structure of waste kelp, its surface has a high pH value, various oxygen-containing functional groups, and numerous hollow holes after pyrolysis [17]. Therefore, waste kelp can be considered as an effective material for the preparation of biochar for application in adsorption of Cr from wastewater.

In the present study, waste kelp was selected as the raw material for biochar preparation, and, subsequently, the performance of the prepared biochar to adsorb Cr(III) from an aqueous solution was investigated. The main purpose of this study was (i) to study the characteristics of biochar derived from marine macro-algae kelp and (ii) to evaluate its potential in removing Cr(III) from aqueous solutions. First, the physical, chemical, and morphological characteristics of biochar, produced by marine macro-algae kelp, were characterized. Secondly, various factors that affect the adsorption capacity of Cr(III) by kelp biochar (KB), including reaction time, initial pH, Cr(III) concentration, competitive ion, and biochar dosage, were evaluated. Finally, the adsorption kinetics model and the isotherms model of Cr(III) by KB were developed for the application.

2. Materials and methods

2.1. Materials

The raw biomass waste kelp for biochar production used in this study was collected from Qinhuangdao city, China. The procedure for preparing KB was as follows: (1) the collected waste kelp was washed thoroughly and dried at the room temperature for 24 h, followed by exsiccated at 70°C for 12 h in a drying oven; (2) crushing the dried kelp to 0.18–1.7 mm-diameter particles using mortar; (3) the crushed dried kelp was pyrolyzed in tube furnace. In the furnace, an appropriate amount of dried kelp was added and heated at 100°C for 2.0 h, after which the heating temperature was raised to 500°C at the rate of 7.0°C/min; this temperature was maintained at this value for 2.0 h. Eventually, the system was cooled down to room temperature. During this procedure, nitrogen gas was constantly fed to the furnace at a rate of 2,500 mL/min to prevent the ignition of organic matter in the furnace; (4) the extracted KB was cleaned with deionized water and dried at 70°C–80°C in the drying oven for 12 h, then sealed in a bag for further use [18]. The aqueous solution used in the experiments was prepared by dissolving $CrCl_3$ into distilled water. The cation stock solutions (5.0 g/L) was used to prepare the working solutions and was composed of KCl, $CaCl_2$, NaCl, and $MgCl_2$ in distilled water. Similarly, the stock solutions of individual anions ($C_5H_7O_5COO^-$, CH_3COO^-, PO_4^{3-}, and SO_4^{2-}) present in the Cr(III) solution were prepared by feeding $C_5H_7O_5COONa$, CH_3COONa, $Na_2HPO_4{\cdot}12H_2O$, and Na_2SO_4 to distilled water. All chemicals used in the study were of analytical grade.

2.2. Characterization of the surface properties

The adsorption saturated biochar [Cr(III) concentration, 25 mg/L; initial pH, 3.5; KB dosage, 0.4 g/L; reaction time, 420 min] was collected and dried in an oven at 80°C for 12 h. The physical appearance of the surface of the raw and saturated KBs was observed under a scanning electron microscopy-energy-dispersive X-ray spectroscopy (SEM-EDS; JSM-6701F, Japan). Moreover, to determine the presence of the functional groups on the characteristic surface of raw and saturated KBs, especially the presence of oxygen-containing functional groups, Fourier transform infrared spectrometer (FTIR; Bruker Vertex 80V, USA) was used to characterize the adsorbents.

2.3. Cr(III) adsorption experiments

The procedures of the adsorption kinetics experiment were as follows: first, 500 mL of the aqueous solution with an initial Cr(III) concentration of 25 mg/L and an initial pH of 3.5 was fed to a 1,000 mL beaker placed on a magnetic stirrer, followed by the addition of KB at a dosage of 0.8 g/L. Next, the mixed solution was stirred for 660 min and 5.0 ml of the samples were withdrawn from the flask at different time intervals and filtered through a 0.22 μm filter for the determination of Cr(III) concentration. Finally, the experimental data were fitted with the pseudo-first-order and second-order models.

The adsorption isotherm experiment was performed in the following manner: initially, 50 mL of the aqueous solution with different initial Cr(III) concentrations (5–40 mg/L) and an initial pH of 3.5 was added to a 100 mL beaker, to which KB was fed at a dosage of 0.8 g/L. Subsequently, the mixed solution was stirred for 420 min, and 10 mL of the samples were removed at the end of the reaction, followed

by filtering through a 0.22 μm filter for the Cr(III) analysis. Finally, the experimental data were fitted with the Langmuir and Freundlich models.

The operating procedures of the influencing experimental conditions were similar to those of the adsorption isotherm experiment. As for the effect of initial pH on Cr(III) removal, the initial concentration of Cr(III) in the solution was 25 mg/L, while the initial pH ranged from 1.0 to 8.0. Furthermore, investigations were performed to determine the effect of the individual cation (K^+, Ca^{2+}, Na^+, and Mg^{2+}) present in the Cr(III) solution on the adsorption by KB. For this purpose, solutions with a Cr(III) concentration of 25 mg/L and individual cation concentrations of 0.0–60.0 mg/L were used. Similarly, the effects of 4 types of anions ($C_5H_7O_5COO^-$, CH_3COO^-, PO_4^{3-}, and SO_4^{2-}) on the removal of Cr(III) by KB were also investigated. In this experiment, the concentrations of anions varied from 0.0 to 6.0 mmol/L. In addition, the effect of KB dosage (0.4–1.6 g/L) on the removal of Cr(III) by KB was investigated at an initial Cr(III) concentration of 25 mg/L and an initial pH of 3.5.

In this study, the Cr(III) concentration was measured using an atomic absorption spectrophotometer (WFX-120; China). The calculation formulas of the capacity and efficiency of Cr(III) adsorbed on KB are given in Eqs. (1) and (2), respectively, as follows:

$$q_t = \frac{(C_0 - C_t)V}{m} \tag{1}$$

$$A = \frac{(C_0 - C_t)}{C_0} \times 100\% \tag{2}$$

where q_t is the adsorption capacity of Cr(III) on biochar (mg/g), A represents the adsorption efficiency (%) of Cr(III) by biochar, C_0 and C_t represent the initial and equilibrium concentrations (mg/L) of Cr(III), respectively, V is the volume of the aqueous solution (L), and m is the mass (g) of biochar.

3. Results and discussion

3.1. Characterization of adsorbent materials

3.1.1. Surface features and interior structure

The functional groups on the surface of biochar play a key role in metal adsorption. The formation of these functional groups mainly depends on the use of specific biomass and pyrolysis temperature [1]. Fig. 1 depicts the FTIR patterns of KB before and after Cr(III) adsorption, suggesting that their spectra were almost similar, albeit the intensity changes were different and band shifts were numerous. The oxygen-containing functional groups such as –OH, C=O, and C–O were observed before and after the KB adsorption [19], and these functional groups can thus play an important role in the binding of heavy metals to biochar [6]. Biochar has broadband at 3,470–3,330 cm^{-1}, which can be attributed to the vibration of the –OH group [20]. In some cases, the –OH group acts as the main binding site for metals owing to the high electronegativity of O. Under this condition, H is released to form the hydrophilic O. Fig. 1 further shows that the –OH broadband after KB adsorption was narrower

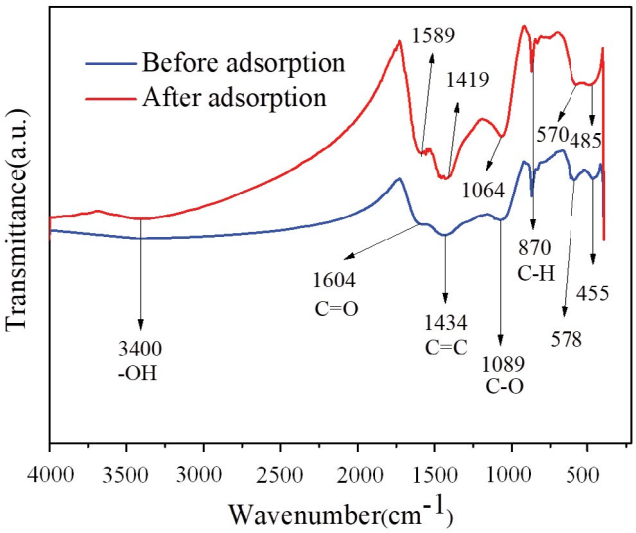

Fig. 1. FTIR spectra of KB before and after Cr(III) adsorption.

than that before adsorption, which suggests that Cr(III) had occupied the adsorption sites of the –OH group. Owing to the presence of carboxylic acid and nitrogen derivatives, the peak at 1,604 cm^{-1} before adsorption was C=O stretching [21], but after the adsorption of Cr(III), the peak position moved to 1,589 cm^{-1} [22]. The corresponding peak at 1,434 cm^{-1} corresponded to C=C, and the position of the peak after the adsorption of Cr(III) moved to 1,419 cm^{-1}. The peak at 1,089 cm^{-1} was attributed to C–O stretching caused by alcohol, ester, ether, and phenol, and moved to 1,064 cm^{-1} after the adsorption of Cr(III). The appearance of the 870 cm^{-1} peak represents the C–H bond of the aromatic or vinyl group and no change in the peak position was observed after the adsorption of Cr(III). Although the sites of the peaks of 578 and 455 cm^{-1} are unknown functional groups, one can observe from the figure that the sites of the peaks after the adsorption of Cr(III) have obvious changes, which are 570 and 485 cm^{-1} respectively. Comparison of the FTIR spectra of KB before and after Cr(III) adsorption shows that the –OH, C=O, C=C, and C–O groups were involved in the binding of Cr(III) to biochar, suggesting the involvement of several oxygen functional groups in the KB to serve as the potential adsorption sites for heavy metals.

3.1.2. Surface morphology and BET of KB

The SEM images of KB before and after Cr(III) adsorption are shown in Fig. 2. The KB in Fig. 2a reveals the cavity distribution with an asymmetric size. The magnified KB (Fig. 2b) has a porous surface with a honeycomb structure and a large pore of size 50–500 nm, which can be utilized as a micropore and mesopore adsorbent. After Cr(III) binding, the surface of KB was found to be partially covered by some substance (Fig. 2c). Compared with that in Fig. 2c, this cover in Fig. 2d was observed more clearly, which further suggests that Cr(III) may be successfully adsorbed on the KB surface. Furthermore, the EDS measurements of KB before and after Cr(III) adsorption were performed to evaluate the chemical composition changes on the KB surface (Table 1). The EDS

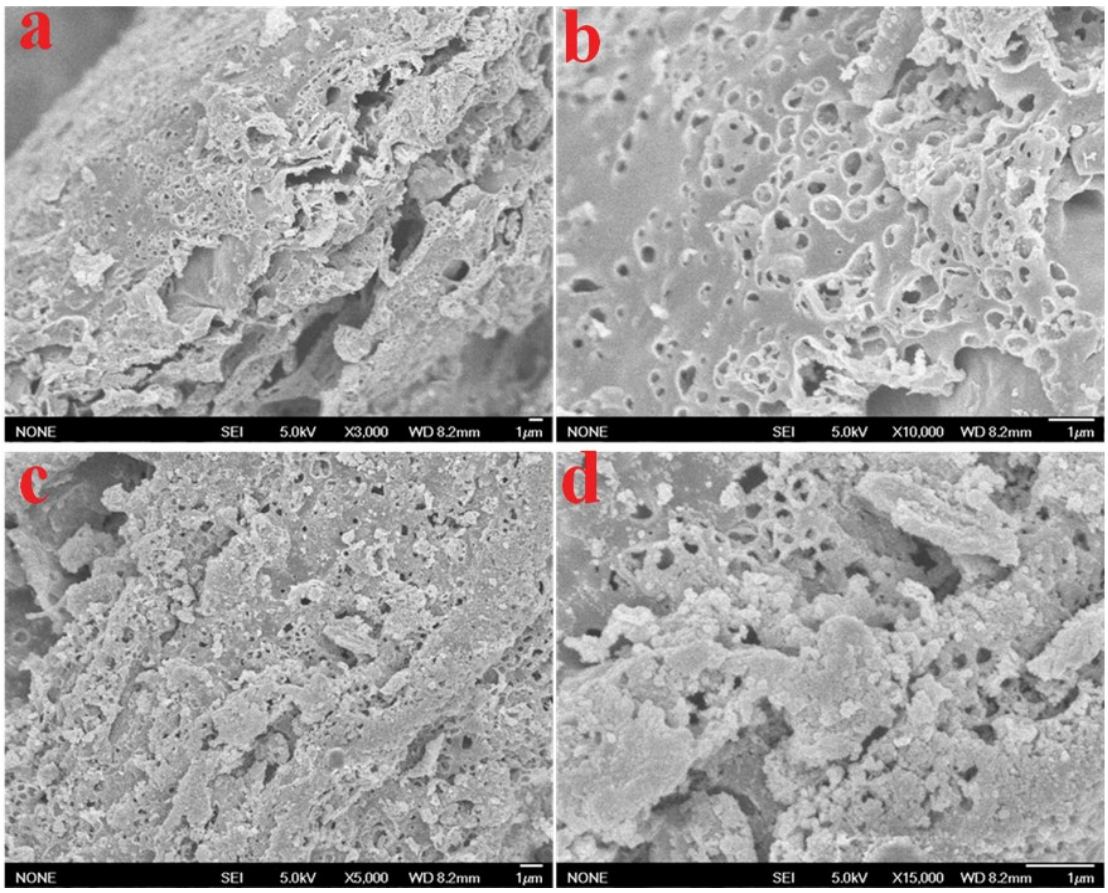

Fig. 2. SEM images of KB (a,b) before adsorption and (c,d) after adsorption.

Table 1
EDS characterization and textural characteristics results of KB before and after adsorption and literature comparison

Biochar	Elemental composition (%, in mass)				O/C molar ratio	Textural characteristics	
	C	O	S	Cr		Barrett–Joyner–Halenda pore surface area (m^2/g)	Adsorption capacity (mg/g)
KB (before adsorption)	64.39	25.32	0.5	0	0.39	14.94	–
KB (after adsorption)	64.49	27.65	0.46	1.26	0.43	17.05	22.63
Biochar made of rice [22]	47.8	10.3	0.5	–	0.23	46.9	1.11 (Hg^0)
Biochar made of tobacco [22]	42.3	15.0	0.5	–	0.35	23.9	3.4 (Hg^0)

results reveal that C (64.39 wt.%) and O (25.32 wt.%) were the main elements on the KB surface without any trace of Cr(III). After the adsorption of Cr(III), as seen in Table 1, the Cr(III) element appeared on the surface of KB, which further corroborates the removal of Cr(III) by the KB. As observed in Table 1, KB has a higher O/C (oxygen/carbon) ratio as compared to traditional rice and tobacco biochar [22]. The O/C ratio can be used as a hydrophilic index. Therefore, a high O/C ratio indicates that an aqueous solution can easily permeate into biochar, which is conducive to the adsorption of Cr(III) on KB.

In addition, as seen in Table 1, in comparison to the biochar made of rice and tobacco, KB has the lowest surface area and the highest adsorption capacity of 22.63 mg/g for Cr(III), which suggests that the surface area is not the decisive factor for a high adsorption rate. The high adsorption capacity of KB may be related to the functional groups and charges present on the surface. After adsorbing Cr(III), the surface area increased from 14.94 to 17.05 m^2/g, which implies that Cr(III) was successfully adsorbed by KB.

3.2. Adsorption kinetics and mechanism

The change in the adsorption efficiency of Cr(III) on the KB over time is shown in Fig. 3. As in the figure, in

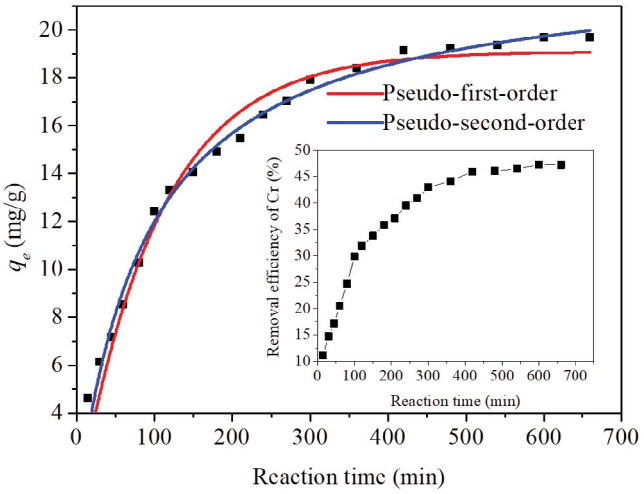

Fig. 3. Adsorption kinetics of chromium adsorption by biochar.

the initial 240 min, the adsorption capacity of Cr(III) on the KB rapidly increased with an increase in time. The rapid adsorption of Cr(III) at this stage may be attributed to the existence of a high driving force for the rapid transfer of Cr(III) onto the surface of the adsorbent particles as well as the possibility of the presence of uncovered surface areas and unoccupied active sites on the adsorbent [23,24]. After 240 min, the adsorption rate of Cr(III) progressively decreased, probably due to the decrease in the availability of the uncovered surface area and the remaining active sites and the decrease in the driving force, which resulted in a longer time requirement by Cr(III) for entering the inner pores of the adsorbent particles [25,26]. The adsorption process of Cr(III) at different reaction times noted in this study was consistent with that in the study of Huang et al. [27]. Based on the results and analysis, the process of adsorption of Cr(III) by the KB can be divided into 3 stages: (i) the rapid adsorption stage at the first 240 min, (ii) the slow adsorption stage during the next 240–420 min, and (iii) the equilibrium stage after 420 min. With the increase in time, the 3 stages were also discovered in the phosphate adsorption by wheat straw biochar [27].

To evaluate the dynamic behavior of Cr(III) adsorption on KB, the kinetic models of pseudo-first-order (Eq. (3)) and second-order (Eq. (4)) [28] were used to fit the experimental data. When the adsorption process is pure physical adsorption, it can be described by the pseudo-first-order kinetic model. However, when it exists as chemical adsorption, which mainly involves the transfer or sharing of electrons, the pseudo-second-order kinetic model can describe it adequately. As follows [29]:

$$q_t = q_e\left(1 - e^{-k_1 t}\right) \tag{3}$$

$$q_t = \frac{k_2 q_e^2 t}{1 + k_2 q_e t} \tag{4}$$

where q_t is the adsorption capacity of Cr(III) at the time t on biochar (mg/g), q_e is the adsorption capacity at the equilibrium state (mg/g), t is the adsorption time (min), and k_1 and k_2 are the rates constant of the pseudo-first-order dynamic model (min^{-1}) and the rate constant of pseudo-second-order dynamic model (g mg^{-1} min^{-1}), respectively.

In this study, the fitting results of pseudo-first-order and pseudo-second-order models are summarized in Table 2. As observed from this table, the pseudo-second-order kinetic model has higher values of coefficient constant R^2 (>0.99) than the pseudo-first-order kinetic model (R^2 > 0.97), suggesting that the pseudo-second-order kinetic model has a better fitting effect and can better describe the adsorption of Cr(III) on KB. The fitting result of pseudo-second-order kinetic model also proves that the adsorption mechanism of Cr(III) on KB is not only attributed to electrostatic adsorption but also chemical adsorption. The high pH at the surface of KB may explain chemical adsorption. Furthermore, the chemical adsorption may be related to the surface charge of KB [30].

3.3. Adsorption isotherms

Fig. 4 illustrates the adsorption isotherm of Cr(III) on KB. As observed in Fig. 3, with an increase in the initial concentration of Cr(III), the adsorption capacity of Cr(III) also progressively increased, which suggests that the concentration gradient was the driving force of Cr(III) adsorption on KB. Higher concentration indicates more opportunities to bind the adsorption sites of KB with Cr(III) ions, which in turn improves the success rate of adsorption. At the tested concentration range, the adsorption capacity of Cr(III) was found to increase rapidly at the Cr(III) concentration of 5–20 mg/L, followed by a slower increase at the concentration of 20–40 mg/L. The above increase may be due to an increase in the Cr(III) concentration. Thus, the Cr(III) adsorption on the KB gradually approached saturation, and the availability of the adsorption sites on the surface of KB rapidly decreased. As seen in Fig. 4, at the Cr(III) concentration of 30–40 mg/L, the adsorption capacity of Cr(III) reached 25 mg/g. The adsorption isotherm for hydrogel has been reported by Jiang et al. and displayed a similar phenomenon to our study [31], indicating that the contaminant concentration is a vital factor for the adsorption process. In the literature, Pan et al. [32] reported that the Cr(III) adsorption capacities of activated carbon, rice straw char, canola straw char, soybean straw char, and peanut straw char were 5, 13, 15, 18, and 24 mg/g, respectively, at the Cr(III) concentration of 1–200 mg/L.

Table 2
Parameters of kinetic models for the adsorption of Cr(III) on the KB

Models	Parameters	Value
Pseudo-first-order model	q_e (mg/g)	19.09
	k_1 (min^{-1})	0.01
	R^2	0.97
Pseudo-second-order model	q_e (mg/g)	22.66
	k_2 (g mg^{-1} min^{-1})	0.05×10^{-2}
	R^2	0.99

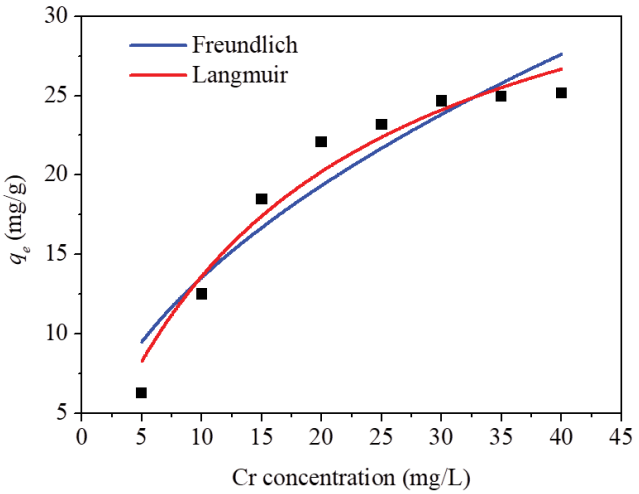

Fig. 4. Adsorption isotherms of Cr(III) adsorbed by biochar at 5–40 mg/L.

To characterize the adsorption equilibrium of Cr(III) by the KB, the Langmuir and Freundlich models [33] were applied to fit the experimental data. The Langmuir isotherm model (Eq. (5)) states that the uniform distribution of adsorption sites and adsorption energy are the same and that each adsorption site allows the adsorption of only one molecule, neglecting the interaction between the adsorbates. Therefore, the Langmuir isotherm model is usually applied to describe monolayer adsorption, as follows [34].

$$q_e = \frac{q_m b C_e}{1 + bC_e} \tag{5}$$

where q_e and q_m are the adsorption capacity at the equilibrium state and theoretical maximum adsorption capacity (mg/g), respectively; b is the Langmuir parameter to evaluate the affinity of Cr(III) ion toward biochar (L/mg), and C_e is the equilibrium concentration of the adsorbate (mg/L).

The linear form of the Freundlich isotherm model is given as follows:

$$q_e = K_F C_e^{1/n} \tag{6}$$

where q_e is the adsorption capacity at the equilibrium state (mg/g), K_F is the Freundlich parameter (L/mg), which indicates the affinity of KB to an adsorbate ion. C_e is the equilibrium concentration of the adsorbate (mg/g), and n is the empirical constant to evaluate the adsorption strength of adsorbent. The Freundlich adsorption isotherm assumes the non-uniform adsorption sites, the different surface energy of adsorbent, and the change in the adsorption heat with the surface coverage. Therefore, the Freundlich model is used to describe the multilayer adsorption behavior of a typical heterogeneous surface [2].

In this study, the nonlinear fitting of experimental data by the Langmuir and Freundlich models was performed, and the fitting results are shown in Fig. 4 and Table 3. Both the illustrations confirm that the Langmuir isothermal model yielded a much better result ($R^2 > 0.95$), which fitted the data

Table 3
Parameters of the adsorption isotherm model for the adsorption of Cr(III) on the KB

Models	Parameters	Value
Langmuir isotherm model	q_m	39.16
	b (L/mg)	0.05
	R^2	0.95
Freundlich isotherm model	K_F	4.15
	n	1.95
	R^2	0.89

in comparison to that of the Freundlich isothermal model ($R^2 > 0.89$). These observations suggested that the Langmuir isothermal model can better represent the adsorption behavior of Cr(III) on the KB as compared to the Freundlich isothermal model, which in turn indicates that KB adsorption was monolayer adsorption and that all of the adsorption sites had an equal solute affinity. The maximum adsorption capacity of Cr(III) by the KB at the equilibrium was 39.16 mg/g, which was higher than that of Cr(III) by the peanut straw biochar (24 mg/g) [32]. Moreover, the n constant of the Freundlich isotherm represents the adsorption affinity of Cr(III) in a solution onto the KB. In this study, the value of n was >1.0, which suggests that the adsorption isotherm is characterized by favorable heterogeneous adsorption. This result is consistent with that reported by Liu et al. [35].

3.4. Effect of initial pH

The effects of initial pH on Cr(III)-removal efficiency and solution pH are shown in Fig. 5a. The removal efficiency of Cr(III) had no significant change at the initial pH of 1–2, but it rapidly increased to 86.53% when the initial pH increased from 3 to 4, and then remained stable at around 85% at the initial pH > 4.0. At a low initial pH, the corresponding low removal capacity of Cr(III) can be attributed to the inhibition of the high concentration of H^+, which may affect the adsorption of Cr(III) by the active sites on the competitive adsorbent material [36]. In addition, H^+ has a great affinity for several complex and ion exchange sites. With an increase of pH, the H^+ concentration decreased, and the active sites of KB increased, which are conducive to the adsorption of Cr(III) [37]. Moreover, anion containing the oxygen functional group can form a surface complex with Cr(III) on biochar. Furthermore, with increasing initial pH, the dissociation of acidic functional groups also increases, which enhances the complexation between Cr(III) and the functional group anions, thereby increasing the specific adsorption of Cr (III) by biochar [32]. Furthermore, it was observed that, at the tested initial pH range, the solution pH after the reaction increased slightly, which may be due to the pH buffer capacity of the biochar [38]. Fig. 5b displays the point of zero charges (pH_{PZC}) to be 2.71. When the pH < pH_{PZC}, the surface charge became positive, leading to an electrostatic repulsion to positively charged Cr(III), which may explain the lack of adsorption of Cr(III) on KB at pH 1–2. However, a progressive increase in the adsorption of Cr(III) at pH > 3 may be attributed to the presence of a negative surface charge, which

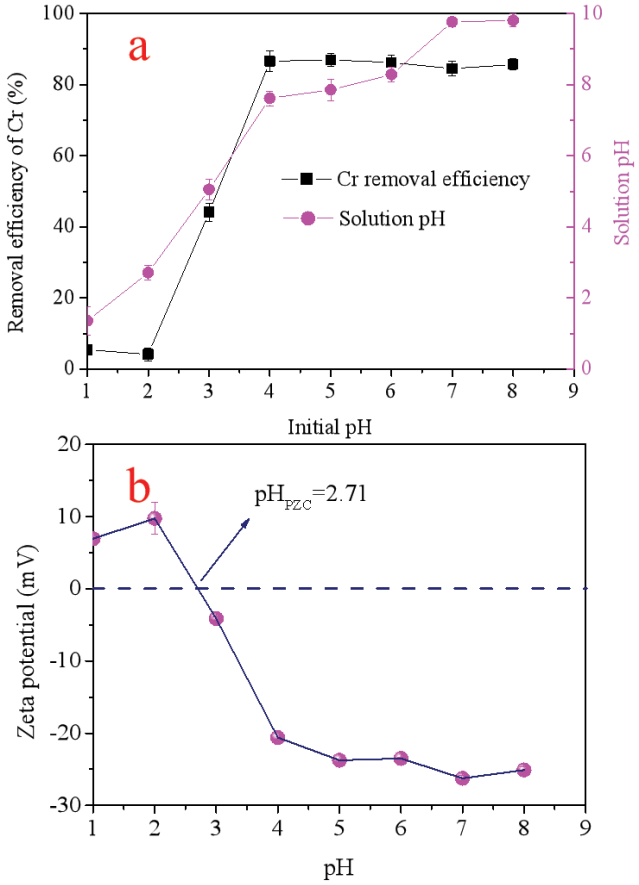

Fig. 5. Effect of pH on adsorption of Cr(III) by KB (a) and zeta potential of KB at different pH (b).

creates an electrostatic attraction for positively charged Cr(III) [39]. Therefore, the adsorption mechanism may be caused by electrostatic interaction and complexation with the functional groups, as also reported by Gutiérrez-Valtierra et al. [40].

3.5. Effect of cations

The experimental results for the adsorption of Cr(III) on the KB in the presence of K^+, Ca^{2+}, Na^+, and Mg^{2+} individually are shown in Fig. 6. From this figure, it can be observed that, when the K^+, Na^+, and Mg^{2+} were present in the solution, these metal cations had almost no effect on the removal of Cr(III) by the KB with the cation concentration increasing from 0 to 60 mg/L. However, when Ca^{2+} was present in the solution, the removal efficiency of Cr(III) by the KB decreased rapidly from 72.50% in the absence of Ca^{2+} to 52.92% in the presence of 60 mg/L of Ca^{2+} ion. The effect of the presence of K^+, Na^+, and Mg^{2+} has two possible explanations. First, the KB could adsorb Cr(III) and 3 other cations simultaneously, which implies that the adsorption capacity of KB was sufficiently strong and there was no competitive adsorption point among the several ions. Second, the affinity of the KB to Cr(III) was higher than those of K^+, Na^+, and Mg^{2+} ions in the solution [41]. As a result, the removal rate of Cr(III) remained stable in the presence of the three cations.

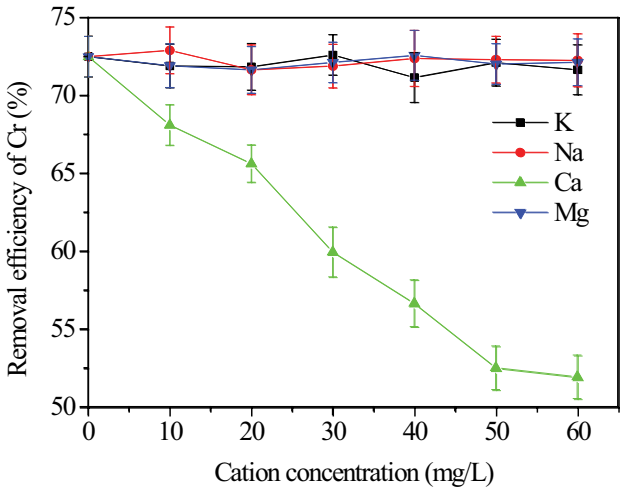

Fig. 6. Effect of cation on adsorption of Cr(III) by KB.

On the other hand, in the presence of Ca^{2+}, the reduction in Cr(III)-removal efficiency may be partly due to the suppression of the attraction between it and the surface of KB, which is the screening effect of surface charges caused by the concentration of Ca^{2+} [42]. In addition, the increase in the concentration of Ca^{2+} may reduce the number of adsorption sites and the affinity of the adsorbent materials.

3.6. Effect of anions

Various anions such as citrate ($C_5H_7O_5COO^-$), acetate (CH_3COO^-), phosphate (PO_4^{3-}), and sulfate (SO_4^{2-}) are often found present in wastewater, which may interfere with the adsorption of Cr(III) by KB. Fig. 7 shows the influence of anion species on Cr(III) removal by the KB. From the figure, one can infer that, when the polyvalent anions PO_4^{3-} and SO_4^{2-} are present in a solution, no obvious effect occurs on the removal efficiency of Cr(III) by the KB. However, the removal efficiency of Cr(III) decreased significantly in the presence of monovalent organic anions. For example, the removal efficiency of Cr(III) decreased from the initial 72.5% to 9.67% and then to 1.66% when the CH_3COO^- and $C_5H_7O_5COO^-$ concentrations increased from 0 to 1 mmol/L, respectively. Fig. 7 also demonstrates that the inhibitory effect of $C_5H_7O_5COO^-$ on the adsorption of Cr(III) by KB was stronger than that of CH_3COO^-. Furthermore, the increase in the monovalent anion concentration could reduce the activity coefficient of Cr(III) and the chance of collision between KB and Cr(III) [43].

3.7. Effect of adsorbent dosage

The results for the effect of KB dosage on the removal of Cr(III) are shown in Fig. 8. This figure elucidates that, when the dosage of KB increased from 0.4 to 0.9 g/L, the removal efficiency of Cr(III) increased sharply from 21.12% to 91.13%, while the adsorption amount increased from 13.20 to 26.70 mg/g. This increase can be further expounded by mentioning that an increase in the amount of adsorbent increases the surface and pore volume of the adsorbent

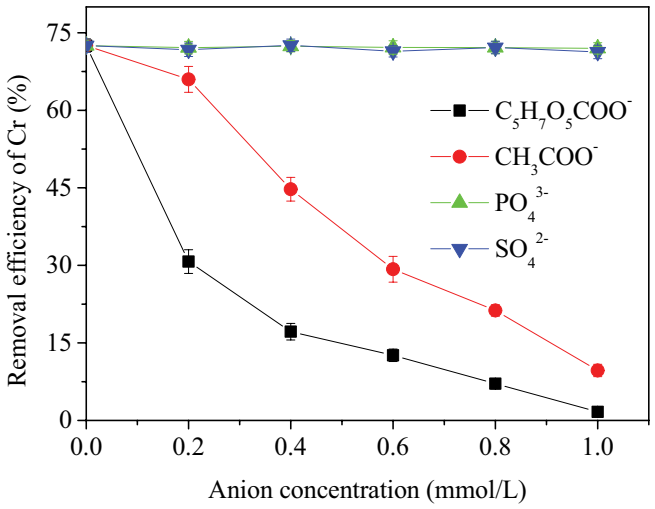

Fig. 7. Effect of anion on adsorption of Cr(III) by KB.

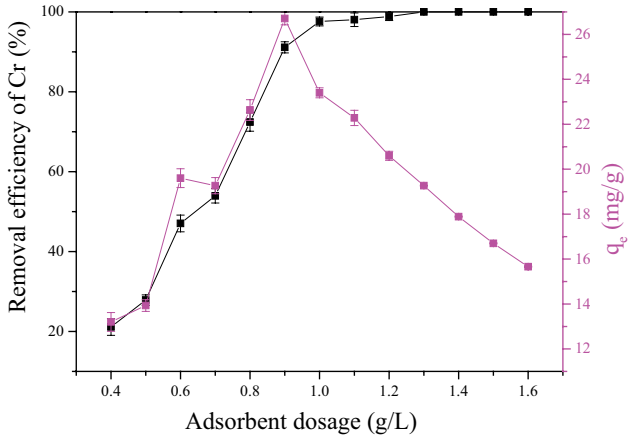

Fig. 8. Effect of KB dosage on adsorption of Cr(III) by KB.

material, thereby providing more functional groups and more active adsorption sites that in turn increase the Cr(III)-removal efficiency [23]. On the other hand, when the amount of the KB increased from 0.9 to 1.6 g/L, only a slight change was noted in the Cr(III)-removal efficiency, although a sharp decrease was noted for the adsorption capacity from 26.70 to 15.65 mg/g. The decrease in the Cr(III) adsorption capacity may be attributed to overcrowding caused by an excessive concentration of the adsorbent [44], which resulted in the formation of aggregates or precipitation of particles. Eventually, by considering the results and analysis, it can be confirmed that 0.9 g/L of KB dosage was optimal for the optimal removal of Cr(III) by the KB.

4. Conclusion

In the present paper, we studied the removal of Cr(III) from an aqueous solution using biochar derived from waste kelp. The following conclusions were drawn.

The FTIR analysis revealed the presence of a large number of oxygen functional groups in KB, which provides potential adsorption sites for the adsorption of Cr(III). The SEM-EDS characterization demonstrated that KB as an adsorbent has a high potential ability. The investigation results of the adsorption isotherms confirmed that the maximum adsorption capacity of Cr(III) by the KB was 39.16 mg/g. Furthermore, KB had a strong adsorption effect on Cr(III) at pH > 3, where the electrostatic interaction and complexation were effective mechanisms of Cr(III) adsorption. When K^+, Ca^{2+}, Na^+, and Mg^{2+} were individually present in the solution, only the presence of Ca^{2+} inhibited the adsorption of Cr(III) on the KB. However, the presence of the polyvalent anions PO_4^{3-} and SO_4^{2-} had no effect on the removal of Cr(III), whereas the presence of the monovalent anions $C_5H_7O_5COO^-$ and CH_3COO^- had an obvious inhibitory effect on KB adsorption of Cr(III). When the dosage of KB was 1.0 g/L, the removal efficiency of Cr(III) by the KB reached 91.13%. Therefore, the present study suggests that KB is an effective adsorbent for removing Cr(III) from an aqueous solution.

Acknowledgments

This work was financially supported by the Natural Science Foundation of Hebei Province (Grant nos. E2018203293) and Qinhuangdao Science and Technology Research and Development Plan (Grant nos. 201801B031).

References

[1] H. Li, X. Dong, E.B. da Silva, L.M. de Oliveira, Y. Chen, L.Q. Ma, Mechanisms of metal sorption by biochars: biochar characteristics and modifications, Chemosphere, 178 (2017) 466–478.
[2] A. Shakya, T. Agarwal, Removal of Cr(VI) from water using pineapple peel derived biochars: adsorption potential and re-usability assessment, J. Mol. Liq., 293 (2019) 111497.
[3] R. Pechancová, T. Pluháček, D. Milde, Recent advances in chromium speciation in biological samples, Spectrochim. Acta, Part B, 152 (2019) 109–122.
[4] Q. Chen, Y. Yao, X. Li, J. Lu, J. Zhou, Z. Huang, Comparison of heavy metal removals from aqueous solutions by chemical precipitation and characteristics of precipitates, J. Water Process Eng., 26 (2018) 289–300.
[5] I.A. Aguayo-Villarreal, A. Bonilla-Petriciolet, R. Muñiz-Valencia, Synthesis of activated carbons from pecan nutshell and their application in the antagonistic adsorption of heavy metal ions, J. Mol. Liq., 230 (2017) 686–695.
[6] T. Wang, H. Sun, X. Ren, B. Li, H. Mao, Adsorption of heavy metals from aqueous solution by UV-mutant *Bacillus subtilis* loaded on biochars derived from different stock materials, Ecotoxicol. Environ. Saf., 148 (2018) 285–292.
[7] D. Pradhan, L.B. Sukla, B.B. Mishra, N. Devi, Biosorption for removal of hexavalent chromium using microalgae *Scenedesmus* sp., J. Cleaner Prod., 209 (2019) 617–629.
[8] X.F. Tan, S.B. Liu, Y.G. Liu, Y.L. Gu, G.M. Zeng, X.J. Hu, X. Wang, S.H. Liu, L.H. Jiang, Biochar as potential sustainable precursors for activated carbon production: multiple applications in environmental protection and energy storage, Bioresour. Technol., 227 (2017) 359–372.
[9] F.R. Oliveira, A.K. Patel, D.P. Jaisi, S. Adhikari, H. Lu, S.K. Khanal, Environmental application of biochar: current status and perspectives, Bioresour. Technol., 246 (2017) 110–122.
[10] L. Lonappan, T. Rouissi, S.K. Brar, M. Verma, R.Y. Surampalli, Adsorption of diclofenac onto different biochar microparticles: dataset - characterization and dosage of biochar, Data Brief, 16 (2018) 460–465.
[11] Y. Deng, S. Huang, D.A. Laird, X. Wang, Z. Meng, Adsorption behaviour and mechanisms of cadmium and nickel on rice straw

biochars in single- and binary-metal systems, Chemosphere, 218 (2019) 308–318.
[12] T. Li, X. Bai, Y.-X. Qi, N. Lun, Y.-J. Bai, Fe_3O_4 nanoparticles decorated on the biochar derived from pomelo pericarp as excellent anode materials for Li-ion batteries, Electrochim. Acta, 222 (2016) 1562–1568.
[13] J. Li, B. Li, H. Huang, N. Zhao, M. Zhang, L. Cao, Investigation into lanthanum-coated biochar obtained from urban dewatered sewage sludge for enhanced phosphate adsorption, Sci. Total Environ., 714 (2020) 136839.
[14] J. Li, B. Li, H. Huang, X. Lv, N. Zhao, G. Guo, D. Zhang, Removal of phosphate from aqueous solution by dolomite-modified biochar derived from urban dewatered sewage sludge, Sci. Total Environ., 687 (2019) 460–469.
[15] K.-m. Jiang, C.-g. Cheng, M. Ran, Y.-g. Lu, Q.-l. Wu, Preparation of a biochar with a high calorific value from chestnut shells, New Carbon Mater., 33 (2018) 183–187.
[16] Y. Wang, R. Liu, H_2O_2 treatment enhanced the heavy metals removal by manure biochar in aqueous solutions, Sci. Total Environ., 628–629 (2018) 1139–1148.
[17] K.M. Poo, E.B. Son, J.S. Chang, X. Ren, Y.J. Choi, K.J. Chae, Biochars derived from wasted marine macro-algae (*Saccharina japonica* and *Sargassum fusiforme*) and their potential for heavy metal removal in aqueous solution, J. Environ. Manage., 206 (2018) 364–372.
[18] H.P. Lu, Z.A. Li, G. Gasco, A. Mendez, Y. Shen, J. Paz-Ferreiro, Use of magnetic biochars for the immobilization of heavy metals in a multi-contaminated soil, Sci. Total Environ., 622–623 (2018) 892–899.
[19] M. Li, H. Liu, T. Chen, C. Dong, Y. Sun, Synthesis of magnetic biochar composites for enhanced uranium(VI) adsorption, Sci. Total Environ., 651 (2019) 1020–1028.
[20] D. Harikishore Kumar Reddy, S.-M. Lee, Magnetic biochar composite: facile synthesis, characterization, and application for heavy metal removal, Colloids Surf., A, 454 (2014) 96–103.
[21] D. Yuan, C. Zhang, S. Tang, X. Li, J. Tang, Y. Rao, Z. Wang, Q. Zhang, Enhancing CaO_2 fenton-like process by Fe(II)-oxalic acid complexation for organic wastewater treatment, Water Res., 163 (2019) 114861.
[22] T. Wang, J. Wu, Y. Zhang, J. Liu, Z. Sui, H. Zhang, W.-Y. Chen, P. Norris, W.-P. Pan, Increasing the chlorine active sites in the micropores of biochar for improved mercury adsorption, Fuel, 229 (2018) 60–67.
[23] Y. Li, Q. Du, X. Wang, P. Zhang, D. Wang, Z. Wang, Y. Xia, Removal of lead from aqueous solution by activated carbon prepared from *Enteromorpha prolifera* by zinc chloride activation, J. Hazard. Mater., 183 (2010) 583–589.
[24] H. Zhao, Y. Lang, Adsorption behaviors and mechanisms of florfenicol by magnetic functionalized biochar and reed biochar, J. Taiwan Inst. Chem. Eng., 88 (2018) 152–160.
[25] G.M. Al-Senani, F.F. Al-Fawzan, Adsorption study of heavy metal ions from aqueous solution by nanoparticle of wild herbs, Egypt. J. Aquat. Res., 44 (2018) 187–194.
[26] M.A. Al-Anber, Removal of high-level Fe^{3+} from aqueous solution using natural inorganic materials: bentonite (NB) and quartz (NQ), Desalination, 250 (2010) 885–891.
[27] Y. Huang, X. Lee, M. Grattieri, M. Yuan, R. Cai, F.C. Macazo, S.D. Minteer, Modified biochar for phosphate adsorption in environmentally relevant conditions, Chem. Eng. J., 380 (2020) 122375.
[28] Q. An, Y.Q. Jiang, H.Y. Nan, Y. Yu, J.N. Jiang, Unraveling sorption of nickel from aqueous solution by $KMnO_4$ and KOH-modified peanut shell biochar: implicit mechanism, Chemosphere, 214 (2019) 846–854.
[29] L. Lu, Y. Lin, Q. Chai, S. He, C. Yang, Removal of acenaphthene by biochar and raw biomass with coexisting heavy metal and phenanthrene, Colloids Surf., A, 558 (2018) 103–109.
[30] Y. Chen, B. Wang, J. Xin, P. Sun, D. Wu, Adsorption behavior and mechanism of Cr(VI) by modified biochar derived from *Enteromorpha prolifera*, Ecotoxicol. Environ. Saf., 164 (2018) 440–447.
[31] C. Jiang, X. Wang, G. Wang, C. Hao, X. Li, T. Li, Adsorption performance of a polysaccharide composite hydrogel based on crosslinked glucan/chitosan for heavy metal ions, Composites Part B, 169 (2019) 45–54.
[32] J. Pan, J. Jiang, R. Xu, Adsorption of Cr(III) from acidic solutions by crop straw derived biochars, J. Environ. Sci., 25 (2013) 1957–1965.
[33] H. Li, J. Xiong, G. Zhang, A. Liang, J. Long, T. Xiao, Y. Chen, P. Zhang, D. Liao, L. Lin, H. Zhang, Enhanced thallium(I) removal from wastewater using hypochlorite oxidation coupled with magnetite-based biochar adsorption, Sci. Total Environ., 698 (2019) 134166.
[34] S. Norouzi, M. Heidari, V. Alipour, O. Rahmanian, M. Fazlzadeh, F. Mohammadi-Moghadam, H. Nourmoradi, B. Goudarzi, K. Dindarloo, Preparation, characterization and Cr(VI) adsorption evaluation of NaOH-activated carbon produced from Date Press Cake; an agro-industrial waste, Bioresour. Technol., 258 (2018) 48–56.
[35] X. Liu, Z.Q. Chen, B. Han, C.L. Su, Q. Han, W.Z. Chen, Biosorption of copper ions from aqueous solution using rape straw powders: optimization, equilibrium and kinetic studies, Ecotoxicol. Environ. Saf., 150 (2018) 251–259.
[36] X. Zhou, J. Zhou, Y. Liu, J. Guo, J. Ren, F. Zhou, Preparation of iminodiacetic acid-modified magnetic biochar by carbonization, magnetization and functional modification for Cd(II) removal in water, Fuel, 233 (2018) 469–479.
[37] F. Xiao, J. Cheng, W. Cao, C. Yang, J. Chen, Z. Luo, Removal of heavy metals from aqueous solution using chitosan-combined magnetic biochars, J. Colloid Interface Sci., 540 (2019) 579–584.
[38] T. Chen, Z. Zhou, R. Han, R. Meng, H. Wang, W. Lu, Adsorption of cadmium by biochar derived from municipal sewage sludge: impact factors and adsorption mechanism, Chemosphere, 134 (2015) 286–293.
[39] L.Y. Gao, J.H. Deng, G.F. Huang, K. Li, K.Z. Cai, Y. Liu, F. Huang, Relative distribution of $Cd(^{2+})$ adsorption mechanisms on biochars derived from rice straw and sewage sludge, Bioresour. Technol., 272 (2019) 114–122.
[40] M. Gutiérrez-Valtierra, C. Salazar-Hernández, J.M. Mendoza-Miranda, E. Elorza-Rodríguez, M.J. Puy-Alquiza, M. Caudillo-González, M.M. Salazar-Hernández, Cr(III) removal from tannery effluents using silica obtained from rice husk and modified silica, Desal. Wat. Treat., 158 (2019) 152–163.
[41] Y. Wu, S. Zhang, X. Guo, H. Huang, Adsorption of chromium(III) on lignin, Bioresour. Technol., 99 (2008) 7709–7715.
[42] H. Zhao, X. Liu, Z. Cao, Y. Zhan, X. Shi, Y. Yang, J. Zhou, J. Xu, Adsorption behavior and mechanism of chloramphenicols, sulfonamides, and non-antibiotic pharmaceuticals on multi-walled carbon nanotubes, J. Hazard. Mater., 310 (2016) 235–245.
[43] Z.-b. Zhang, X.-h. Cao, P. Liang, Y.-h. Liu, Adsorption of uranium from aqueous solution using biochar produced by hydrothermal carbonization, J. Radioanal. Nucl. Chem., 295 (2012) 1201–1208.
[44] V.K. Garg, R. Gupta, A. Bala Yadav, R. Kumar, Dye removal from aqueous solution by adsorption on treated sawdust, Bioresour. Technol., 89 (2003) 121–124.